RSC Advances

ROYAL SOCIETY OF CHEMISTRY

www.rsc.org/advances

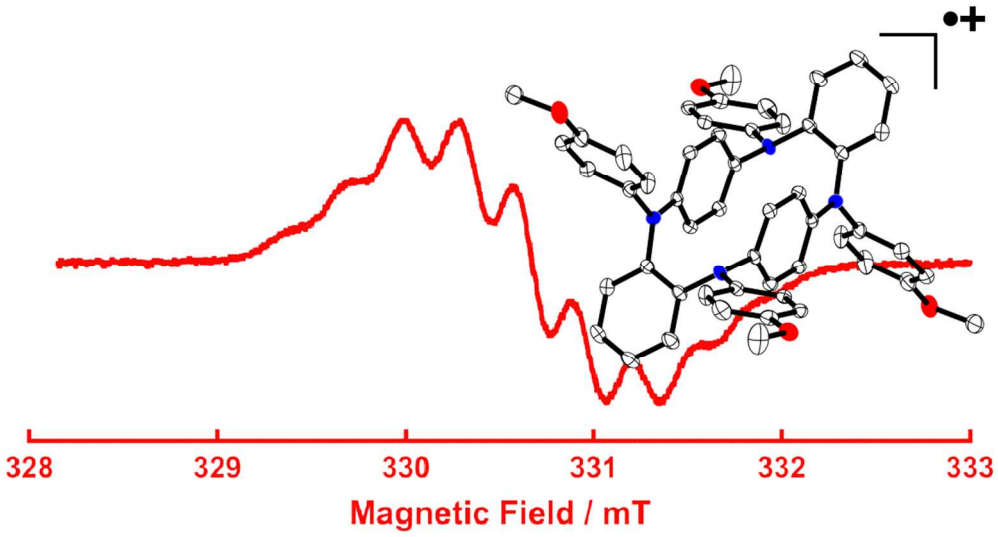

99x54mm (300 x 300 DPI)

Electronic structure of tetraaza[1.1.1.1]*o*,*p*,*o*,*p*-cyclophane and its oxidized states†

Daisuke Sakamaki,[ac] Akihiro Ito,*[a] Takashi Matsumoto[b] and Kazuyoshi Tanaka*[a]

[a] *Department of Molecular Engineering, Graduate School of Engineering, Kyoto University, Nishikyo-ku, Kyoto 615-8510, Japan. E-mails: aito@scl.kyoto-u.ac.jp; ktanaka@moleng.kyoto-u.ac.jp*

[b] *X-ray Research Laboratory, Rigaku Corporation, Matsubara-cho 3-9-12, Akishima, Tokyo, 196-8666, Japan*

[c] *Current address: Department of Applied Chemistry, Graduate School of Engineering,Osaka University, Suita 565-0871, Japan*

† Electronic supplementary information (ESI) available: Experimental details on synthesis, characterizations, theoretical calculations. See DOI: 10.1039/xxxxxxxxxx

Abstract

From the structural point of view, the smallest macrocyclic oligoarylamine bearing the alternant *ortho*-*para*-linkage, tetraaza[1_4]*o*,*p*,*o*,*p*-cyclophane, can be considered as an intriguing compound: two *para*-phenylenediamine (*para*-PD) redox-active units are rigidly fixed in close proximity, being reminiscent of [2.2]paracyclophane. The electrochemical, spectroelectrochemical and ESR spectroscopic studies revealed that the present overcrowded redox-active macrocycle increased its rigidity with increasing the degree of oxidation with the assistance of complementary quantum chemical study. In the radical cation of the macrocycle, very fast dynamic spin (or charge) transfer between the neutral and oxidized *para*-PD units via the *ortho*-phenylene π-bridges was observed in the measured temperature range, while the static spin-delocalization took place within a single *para*-PD unit.

Introduction

Macrocyclic oligoarylamines, *i.e.*, aza[1_n]cyclophanes,[1–4] have been revealed to be an attractive class of macrocyclic compounds, in which the multi-redox activity is given by the introduction of electron-rich nitrogen atoms replacing the methylene linkages between arene rings. Interest in these compounds extends from supramolecular chemistry, where their ability of self-assembly as well as the size and nature of their cavity can be tuned,[1,2,4] to materials chemistry, where the localization and/or delocalization of charges generated by hole-doping process is closely related to their conducting and magnetic properties.[3,5]

Thanks to the synthetic availability by the recent progress on palladium-catalyzed aryl amination reactions,[6–9] a variety of aza[1_n]cyclophanes with different arene-bridged patterns have been reported so far (Chart 1). All kinds of macrocycles with the single substitution pattern, aza[1_n]metacyclophanes (**1**),[10–22] aza[1_n]paracyclophanes (**2**),[23,24] and aza[1_n]orthocyclophanes (**3**)[25] were prepared to investigate spin-spin correlation in cyclic multi-spin systems, delocalization of the polaron generated in linear oligoanilines without chain ends, and possibility for new scaffold in supramolecular chemistry, respectively. In addition, tetraza[1_4]*m*,*p*,*m*,*p*-cyclophane (**4**), the smallest macrocyclic oligoarylamine bearing the alternating *meta–para*-linkage, and the extended congeners are appealing since the rigidity and stability of their toroidal multi-spin systems are indispensable for useful building blocks in magnetic materials.[26–33]

On the other hand, tetraaza[1_4]*o*,*p*,*o*,*p*-cyclophane (**5**), the smallest macrocyclic oligoarylamine bearing the alternant *ortho-para*-linkage, is hitherto unknown in the azacyclophane family.[34] From the structural points of view, macrocycle **5** can be

considered as an intriguing compound: two *para*-phenylenediamine (*para*-PD) redox-active units are rigidly fixed in close proximity reminiscent of the arrangement of the benzene rings in the skeleton of [2.2]- or [3.3]paracyclophanes.[35,36] As a consequence of such a rigid molecular geometry, **5** and its oxidized species are expected to exhibit an interesting electronic structure, probably due to steric constraints between *para*-PD redox-active units clipped together by *ortho*-phenylene, as compared with *meta–para*-linked tetraazacyclophane **4**, in which the distance between the confronting *para*-PD faces (~5Å) are too long to undergo the interannular interaction.[26,28] In this article, we will report on the electronic structure peculiar to its rigid and overcrowded molecular structure of **5**.

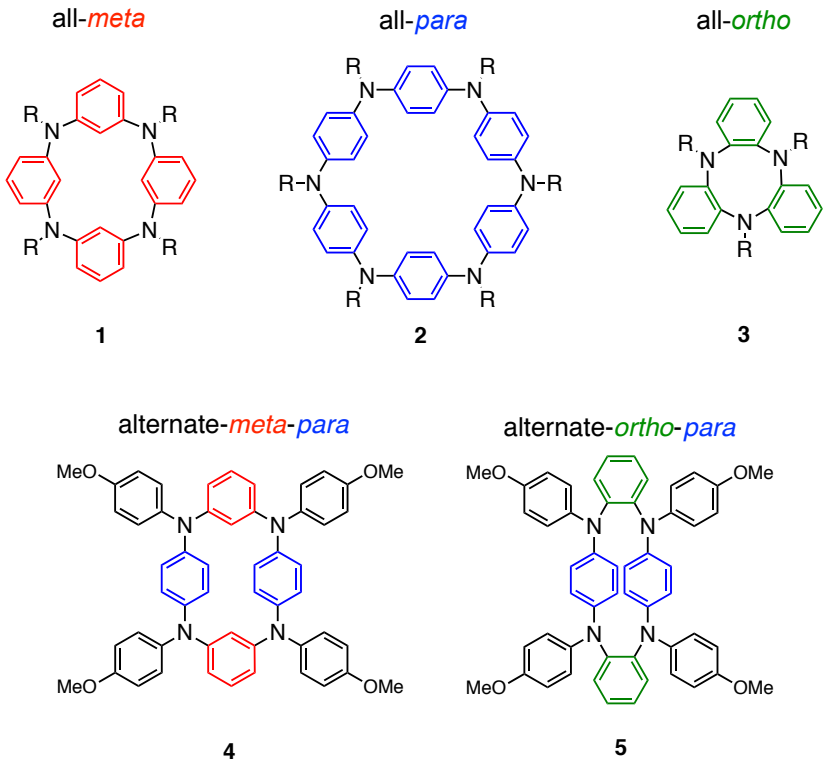

Chart 1 A family of azacyclophanes: tetraaza[1_4]metacyclophane **1**, hexaaza[1_6]paracyclophane **2**, triaza[1_3]orthocyclophane **3**, tetraaza[1_4]*m*,3*p*,*m*,*p*-cyclophane **4**, and tetraaza[1_4]*o*,*p*,*o*,*p*-cyclophane **5**.

Results and discussion

The sign of rigid molecular structure of **5** appeared in the ^{1}H and ^{13}C NMR spectra. For instance, five proton signals are expected in the aromatic region of ^{1}H NMR spectrum, assuming both rapid rotation of *para*-PD units and rapid flipping motion of *ortho*-phenylene linkers of **5** at room temperature. However, the observed ^{1}H NMR spectrum of **5** in [D_6]acetone at 298 K displayed the existence of 12 types of aromatic protons (Fig. 1). This spectrum can be reasonably explained by assuming the existence of two conformers: a chair form and a boat form (Chart 2). Judging from the splitting patterns, a set of signals with large intensity are assignable to the boat conformer, while a set of weak signals to the chair conformer (Fig. 1).[37] The integral of the corresponding aromatic signals gave a conformer ratio at 298 K (boat : chair = 69 : 31), and the energy difference between the two conformers was estimated to be 0.48 kcal mol^{-1} at 298 K, assuming that the conformer ratio is amenable to the Boltzmann distribution. In addition, the ^{13}C NMR spectrum of **1** exhibited not 9-line but 20-line signals in the aromatic region, and this is again explainable by the existence of the two conformational isomers. In contrast, tetraaza[1_4]*m,p,m,p*-cyclophane **4** exhibited a simplified ^{1}H NMR spectrum indicating rapid flipping motion of *meta*-phenylene rings connecting two *para*-PD units. Therefore, these findings strongly suggest the rigidity of the macrocyclic structure of **5**.

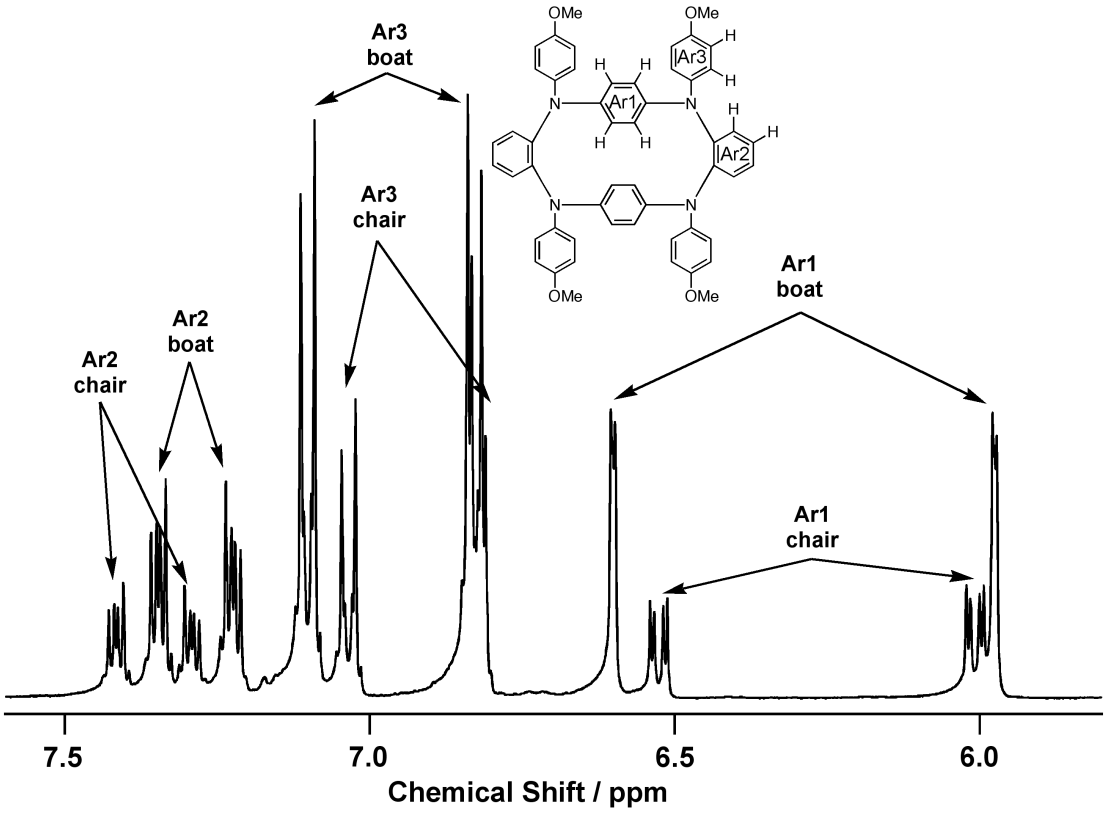

Fig. 1 ^{1}H NMR spectrum in the aromatic region of **5** in [D_6]acetone at 298 K.

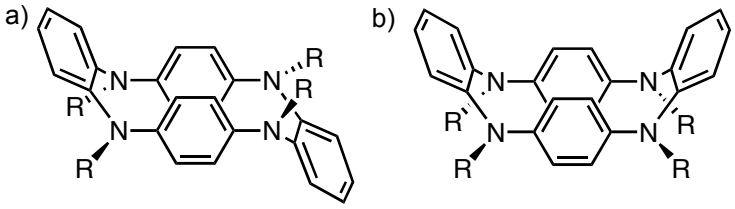

Chart 2 Two conformers of **5** (R = anisyl): a) chair form and b) boat form.

Variable temperature ^{1}H NMR spectroscopic studies of **5** in [D_6]DMSO solution were performed to obtain information about the chair-to-boat conformational change in the temperature range from 298 K to 423 K (ESI Fig. S1†). As the temperature was increased to 383 K, all the signals gradually broadened, and finally, twelve distinct aromatic signals corresponding to both conformers coalesced into broad six ones at 423

K, except for the partial coalescence of the aromatic signals for the *N*-anisyl groups, indicating that rapid chair-to-boat flipping motion takes place. It should be noted that two kinds of aromatic signals for *para*-PD units do not merged into one even at 423 K, providing strong evidence for the rigidity of **5**. The free energy of activation for the chair-to-boat conformational change was estimated as 22 kcal mol^{-1},[38,39] which is comparable to that for the sumanene molecule as a bowl-shaped fullerene fragment.[40] Moreover, decreasing the temperature from 423 K to 298 K showed complete recovery of the original spectrum observed at 298 K (ESI Fig. S1†).

Slow evaporation of a dilute mixed solution (methanol/acetone) of **5** produced purple block crystals suitable for X-ray diffraction (CCDC 956891 contains the supplementary crystallographic data of **5**). Compound **5** crystallized in the triclinic system with space group $P\bar{1}$ with two independent macrocycles per unit cell, and each molecule of **5** was associated with two disordered acetone molecules. The chair conformer was exclusively found in the crystalline state of **5**, whereas the boat conformer was energetically stable as compared with the chair conformer in solution. Two crystallographically independent molecules of **5** adopted structurally very similar chair-shaped conformations with C_i symmetry (Fig. 2; ESI Fig. S2 and Table S2†). Two *para*-phenylene rings were slightly warped, and cofacially stacked to each other. The interannular distance between these two benzene rings were about 3.2 Å, and such a close proximity can afford the through-space charge and/or energy transfer as is the case of the [2.2]paracyclophane (2.83 ~ 3.09 Å)[35] and [3.3]paracyclophane (3.14 ~ 3.31 Å).[36] More noteworthy is that two C-N bond lengths in the *para*-PD unit differ considerably [1.399(3) and 1.445(3) Å for the molecule in Fig. 2 (1.397(3) and 1.436(3) Å for another crystallographically independent molecule)], probably due to the steric

constraints induced by the macrocyclic structure of **5**. As is shown schematically in Fig. 2(b), two nitrogen pseudo-sp^2-planes in **5** were almost coplanar to the *para*-phenylene π-face (an effective π-conjugation with *para*-phenylene), while the other two nitrogen pseudo-sp^2-planes almost perpendicular to the *para*-phenylene π-face (weak π-conjugation). This situation inevitably leads to the shorter and longer C–N bond lengths, respectively.

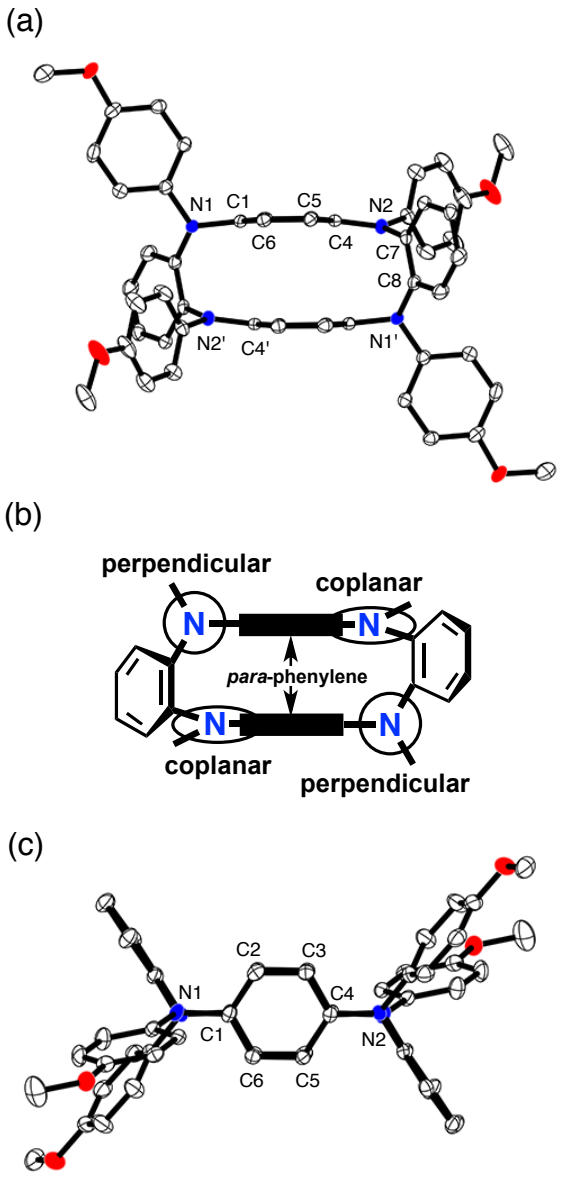

Fig. 2 ORTEP representation of **5** (one of the two crystallographycally independent

molecules): a) top view and b) its schematic drawing (see text), and c) side view. Acetone molecules and hydrogen atoms are omitted for clarity; nitrogen and oxygen atoms are colored in red and blue, respectively; ellipsoids are set at 50% probability. Selected bond lengths (Å) are given: N(1)–C(1) 1.445(3), N(2)–C(4) 1.399(3), C(1)–C(2) 1.388(4), C(2)–C(3) 1.387(3), C(3)–C(4) 1.405(4), C(4)–C(5) 1.407(4), C(5)–C(6) 1.390(3), C(1)–C(6) 1.393(4), N(2)–N(7) 1.433(3), C(7)–C(8) 1.406(4), N(1)'–C(8) 1.423(3), C(1)–C(4)' 3.185(4).

In parallel to the X-ray analysis, the DFT calculations were carried out on a model compound **5**' without methoxy groups in C_i symmetry and the optimized parameters for the two C–N bond lengths in the *para*-PD unit are summarized in Table S3 in the ESI.[41] At present, all the functional tested by using the 6-31G* basis set[42] gave a tendency to underestimate the difference between the two C–N bonds, although the optimized structure for the chair conformer reproduced the structural features of the X-ray structure in all the functionals including M06-2X[43] and ωB97X-D,[44] which were developed to improve the accuracy for describing non-bonding medium range intramolecular interactions. In addition, the B3PW91[45] functional and the local spin density (LDA) functional (SVWN5)[46] did not show better performance for **5**', although those functionals provided the best results for specific cyclophane molecules.[47,48] As has been frequently pointed out recently, the popular B3LYP[49] can lead to a relatively poor description also in the case of compound **5**', in which two benzene rings are stacked within the van der Waals contact (3.4 Å). However, despite these moderate results for all the functionals tested in the present study, at the B3LYP/6-31G* level, the boat conformer with C_1 symmetry was calculated to be slightly stable by 0.26 kcal mol^{-1}, as compared to the chair conformer with C_i symmetry, thus indicating a good agreement with the ^{1}H NMR measurement. In addition, as is described later, time-dependent DFT (TD-DFT[50]) calculations with the B3LYP functional were also satisfactory for

assignment of the lowest energy bands observed in absorption spectra for $\mathbf{5}^{\bullet+}$ and $\mathbf{5}^{2+}$. Hence, as a result of the present benchmark study, we have employed the B3LYP functional for the theoretical considerations of **5**' and its oxidized species.

The redox behavior of **5** was investigated by both the cyclic and differential pulse voltammetries in CH_2Cl_2 (0.1 M tetra-*n*-butylammonium tetrafluoroborate, 100 mV s^{-1}) at 298 K. As shown in Fig. S11 in the ESI†, **5** showed three one-electron redox couples, and the shape of the voltammogram remained unchanged after repeated potential cycling. The large splitting between the first and second oxidation potentials [E_{ox}^{1} = –0.087 V, E_{ox}^{2} = +0.255 V, $\Delta E \equiv E_{ox}^{2} - E_{ox}^{1}$ = 342 mV] suggests the stability of generated radical cation of **5** due to the extension of spin distribution over two *para*-PD units. Furthermore, the ΔE value of **5** is larger than that of tetraaza[1_4]*m,p,m,p*-cyclophane **4** [E_{ox}^{1} = –0.01 V, E_{ox}^{2} = +0.22 V, ΔE = 230 mV],[30] indicating that the replacement of the *meta*-phenylene linkers with the *ortho*-phenylene linkers strengthens the electronic communication between two *para*-PD units. On the other hand, although **5** has four nitrogen atoms, the redox process corresponding to the removal of the forth electron was not observed in CV of **5**, and this is probably because the strong electrostatic repulsion within the overcrowded structure of **5** prohibits the generation of the tetracationic state of **5**.

In order to clarify the electronic structure of $\mathbf{5}^{\bullet+}$, the absorption spectral change upon electrochemical oxidation was measured by using an optically transparent thin-layer electrochemical cell. Fig. 3(a) shows the spectral changes during the oxidation process from **5** to $\mathbf{5}^{\bullet+}$. In this oxidation process, a new absorption band with a asymmetrical band shape appeared at 1.43 eV (λ_{max} = 865 nm) and grew with a slight red shift to 1.38 eV (λ_{max} = 897 nm). During further oxidation to $\mathbf{5}^{2+}$, the absorption band at 1.38 eV

kept on growing with a shoulder at ca. 0.6 eV until the intensity reached up to about twice that of the observed band for $\mathbf{5}^{\bullet+}$ (Fig. 3(b)). What has to be noticed here is that the lowest energy band of $\mathbf{5}^{\bullet+}$ and $\mathbf{5}^{2+}$. To understand the origin of these bands, we carried out time-dependent density functional theory (TD-DFT)[50] calculations (B3LYP/6-31G*) on the model compound of $\mathbf{5}^{\bullet+}$ without methoxy groups.

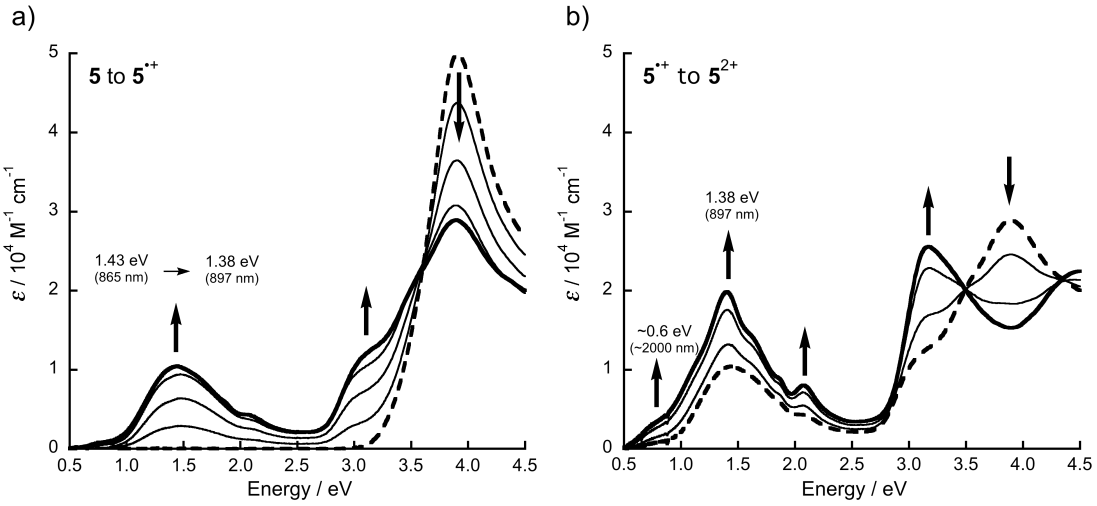

Fig. 3 UV/Vis-NIR absorption spectra of the stepwise electrochemical oxidation of **5** in CH_2Cl_2 with 0.1 M nBu$_4$NBF$_4$ at 298 K: a) **5** (broken line) to $\mathbf{5}^{\bullet+}$ (bold line); b) $\mathbf{5}^{\bullet+}$ (broken line) to $\mathbf{5}^{2+}$ (bold line).

First of all, the geometrical optimizations for two conformers (the boat and chair conformers) of the radical cation ($\mathbf{5'}^{\bullet+}$) have been performed to estimate the relative energy between them. As a consequence, it was found that each conformer has two local minimum structures with different spin (or positive charge) disrtibutions at the B3LYP/6-31G* level: (i) a structure with localized spin (or positive charge) on a single *para*-PD unit, which is referred to as spin-localized structure, and (ii) a structure with delocalized spin over two *para*-PD units, which is referred to as spin-delocalized structure. For the boat conformer, spin-localized and spin-delocalized structures were

predicted to be virtually degenerate. However, when we utilize the M06-2X[43] and ωB97X-D.[44] functionals, it was confirmed that the spin-delocalized structure is converged into a local minimum corresponding to the spin-localized structure. Thus, it can be safely said that the spin-localized structure is the most stable for the boat conformer of **5**''$^{\bullet+}$. On the contrary, for the chair conformer, the spin-localized structure was calculated to be stable as compared with the spin-delocalized structure by 1.05 kcal mol^{-1}. More importantly, it was predicted that the energy difference between the boat and chair conformers increased going from **5**' (0.26 kcal mol^{-1}) to **5**''$^{\bullet+}$ (1.4 kcal mol^{-1}). Thus, the contribution of the boat conformer should be more pronounced in comparison to the chair conformer. As shown in Fig. 4(a), in the spin-localized boat conformer, the C–N bond lengths (1.372 and 1.385 Å) in the positively charged *para*-PD unit were significantly shortened as compared to those (1.428 and 1.431 Å) in the opposite *para*-PD unit, and hence, it is inferred that the positively charged *para*-PD unit adopts a slightly bent semi-quinoid structure.

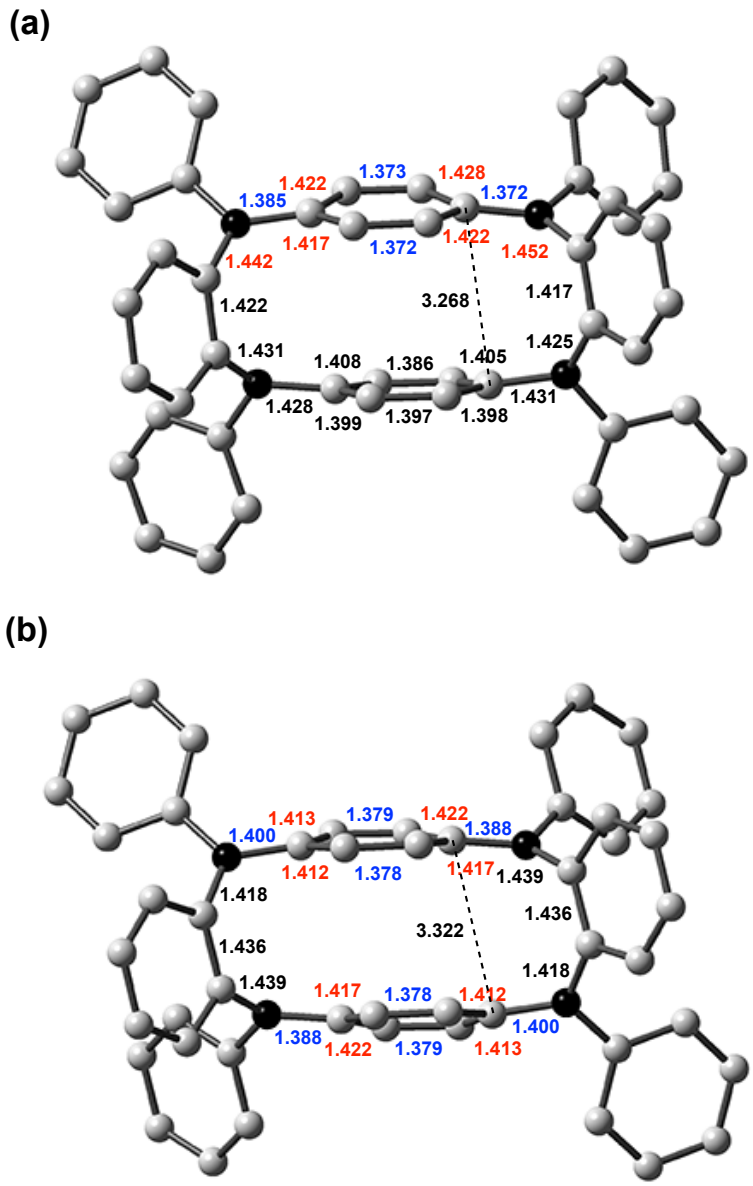

Fig. 4 B3LYP-optimized structures for (a) the spin-localized boat conformer of $\mathbf{5'}^{\bullet+}$ and (b) the boat conformer of $\mathbf{5'}^{2+}$. Bond lengths are shown in Å. The shorter and longer bond lengths in semi-quinoid *para*-PD unit are colored in blue and red, respectively.

As is listed in Table 1, it was found that the TD-DFT-calculated results based on the spin-localized structure of $\mathbf{5}'^{\bullet+}$ qualitatively elucidated the lowest energy band observed for $\mathbf{5}^{\bullet+}$. In addition, the reasonable transition energy was not obtained from the TD-DFT calculations on the spin-delocalized structure. On the basis of the computed Kohn-Sham orbital diagram shown in Fig. 5, the observed lowest-energy band for $\mathbf{5}'^{\bullet+}$ is assignable to the statically delocalized Robin and Day's class III intervalence transition (or charge-resonance band)[51,52] whithin a single *para*-PD unit (β((HO-2)MO) to β(LUMO)). The charge (or spin) transfer band between the adjacent neutral and oxidized *para*-PD units via two *ortho*-phenylene linkers is predicted to be virtually forbidden transition (β(HOMO) to β(LUMO): hν = 0.21 eV; f = 0.0001).

Table 1 TD-DFT calculations of the lowest energy excitation energies for $\mathbf{5}'^{\bullet+}$ and $\mathbf{5}'^{2+}$

species	$h\nu$ (obs) (eV)	calcd $h\nu$ (eV) (f)	assignment
$\mathbf{5}^{\bullet+}$	1.43 (865 nm)	———	
$\mathbf{5}'^{\bullet+}$			
spin-localized chair		1.60 (0.289)	β-(HO–2)MO → β-LUMO
spin-delocalized chair		1.05 (0.296)	β-(HO–1)MO → β-LUMO
spin-localized boat		1.56 (0.312)	β-(HO–2)MO → β-LUMO
spin-delocalized boat		1.25 (0.302)	β-(HO–1)MO → β-LUMO
$\mathbf{5}^{2+}$	~0.6 (sh), 1.38 (897 nm)	———	
$\mathbf{5}'^{2+}$			
chair		0.85 (0.086)	β-HOMO → β-LUMO
		1.54 (0.560)	β-(HO–1)MO → β-LUMO
boat		0.61 (0.074)	β-HOMO → β-LUMO
		1.58 (0.632)	β-(HO–1)MO → β-LUMO

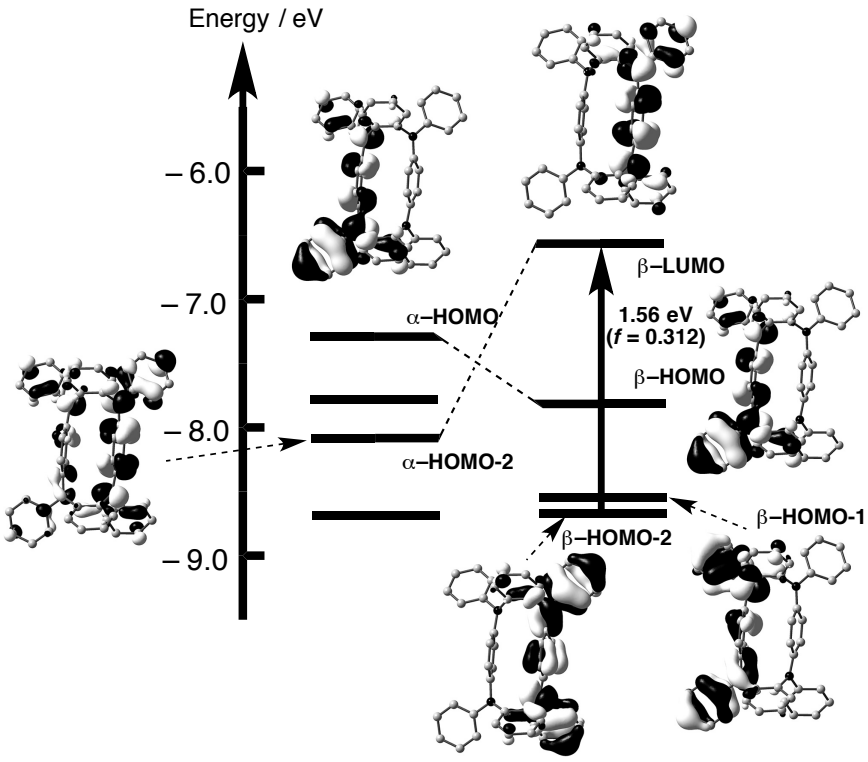

Fig. 5 Frontier Kohn-Sham orbital energy levels for the spin-localized boat conformer of $\mathbf{5}'^{\bullet+}$ at the UB3LYP/6-31G* level of theory. The arrow represents the major contribution to the observed lowest energy transition.

In contrast to the DFT-optimized asymmetrical spin-localized structure for $\mathbf{5}'^{\bullet+}$, all the *para*-PD moieties were predicted to have a semi-quinoid structure in the B3LYP/6-31G* optimizations for two conformers of the dication ($\mathbf{5}'^{2+}$), closely relating to the fact that both *para*-PD units are equally charged by two-electron oxidation of **5**'. In fact, we could not found any local minimum structures with charge localization for both of the two conformers for $\mathbf{5}'^{2+}$. More noteworthy is that the energy difference between the boat and chair conformers further increased going from $\mathbf{5}'^{\bullet+}$ (1.4 kcal mol^{-1}) to $\mathbf{5}'^{2+}$ (4.8 kcal mol^{-1}). This strongly suggests that we can virtually ignore the contribution of the chair conformer in the absorption spectrum observed for $\mathbf{5}^{2+}$. As is

apparent in Fig. 4(b), both of the two *para*-PD units in the boat conformer of $\mathbf{5}'^{2+}$ adopt a same semi-quinoid structure.

Table 1 shows that the lowest energy band observed for $\mathbf{5}^{2+}$ is again qualitatively explainable by the TD-DFT-calculated transition energy based on the most stable structure with boat conformation of $\mathbf{5}'^{2+}$: the observed band can be regarded as an overlap of two transitions, and the value of oscillator strength for the major transition is doubled, as compared to $\mathbf{5}'^{\bullet+}$. On the basis of the computed Kohn-Sham orbital diagram shown in Fig. 6, the observed lowest energy band for $\mathbf{5}^{2+}$ is again assignable to the statically delocalized Robin and Day's class III intervalence transition (or charge-resonance band)[51,52] whithin each *para*-PD unit (from β(HOMO) to β(LUMO) and from β((HO-2)MO) to β(LUMO)).

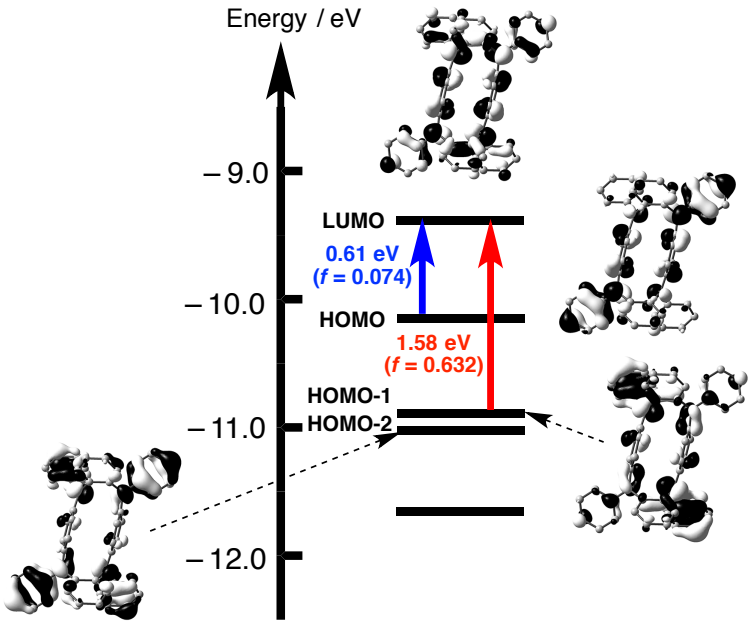

Fig. 6 Frontier Kohn-Sham orbital energy levels for the boat conformer of $\mathbf{5}^{\prime 2+}$ at the B3LYP/6-31G* level of theory. The blue and red arrows represent the major contribution to the lowest and next-lowest energy transitions, respectively.

To gain a direct information on the spin distribution in the MV state of $\mathbf{5}^{\bullet+}$, we recorded the ESR spectrum of $\mathbf{5}^{\bullet+}$ generated by chemical oxidation with 0.5 equiv of tris(4-bromophenyl)aminium hexachloroantimonate (Magic Blue) in CH_2Cl_2. As shown in Fig. 7, a nine line spectrum was observed at 293 K. This spectrum of $\mathbf{5}^{\bullet+}$ was well simulated by the following hyperfine coupling constants: $|a_N|$ = 0.300 mT (4N) and the contribution from unresolved 24 hydrogen nuclei belonging to two *para*-phenylene moieties in the macrocycle (8H) and the benzene rings of four substituted anisyl groups (16H), which were incorporated in the linewidth of the spectral simulation (0.045 mT). Thus, the observed ESR spectrum of $\mathbf{5}^{\bullet+}$ proved that the unpaired electron was dynamically delocalized over the entire macrocyclic molecular backbone on the ESR time scale. In addition, the ESR spectral shape for $\mathbf{5}^{\bullet+}$ remained unchanged in the

measured temperature range from 293 K to 213 K (ESI Fig. S12†). More noteworthy is that the equivalent spin distribution over the four nitrogen nuclei in $\mathbf{5}^{\bullet+}$ demonstrates that an interconversion between the semiquinoidal *para*-PD radical cation unit and the neutral *para*-PD unit takes place very rapidly (the interconversion rate is estimated to be equal to or larger than 10^{10} s^{-1}) in the measured temperature range (Chart 3). Unfortunately, the ESR spectrum reported for $\mathbf{4}^{\bullet+}$ was too unresolved to extract the information on spin distribution.[28]

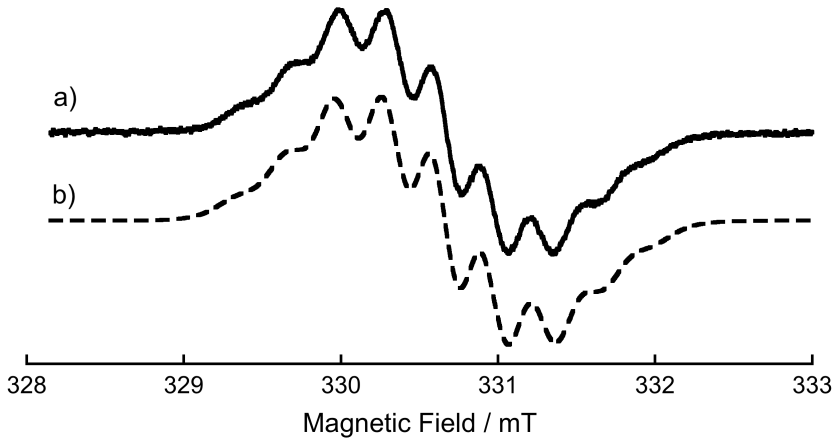

Fig. 7 a) Observed X-band ESR spectrum of $\mathbf{5}^{\bullet+}$ recorded in CH_2Cl_2 at 298 K. b) Simulated ESR spectrum of $\mathbf{5}^{\bullet+}$.

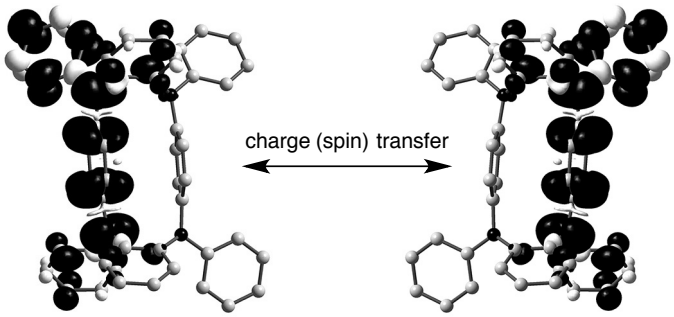

Chart 3 Computed spin density distribution (black: positive spin, white: negative spin; spin isosurface value = 0.001 electron/au^3; UB3LYP/6-31G*) for the spin-localized boat conformation of $\mathbf{5}^{\bullet+}$, and interconversion between the semi-quinoidal *para*-PD radical cation unit and the neutral *para*-PD unit in $\mathbf{5}^{\bullet+}$.

When **5** was treated with 2 equiv of the Magic Blue, the ESR signal almost disappeared, thus indicating the generated dication $\mathbf{5}^{2+}$ is diamagnetic. This result contrasts with the spin triplet state of $\mathbf{4}^{2+}$. However, the diamagnetic electronic structure of $\mathbf{5}^{2+}$ is predictable from the viewpoints of (i) the McConnell-I model,[53,54] where allocation of opposite spin densities between contiguous atoms belonging to each π-face of *para*-PD units results in antiferromagnetic interaction in an eclipsed fashion as shown in Fig. 4(b) and (ii) the topological spin-alignment model,[53,34] represented by Mataga and others, where *ortho*-phenylene can be considered as an anti-ferromagnetic coupling unit.

The influence of the closely π-stacked benzene rings on the electronic properties of **5** can be evaluated also by fluorescence spectroscopy. Although the fluorescence quantum yield was quite low, the fluorescence spectrum of **5** was measured in solution. For comparison, the fluorescence spectra of tetraaza[1_4]*m,p,m,p*-cyclophane **4** and *N,N,N′,N′*-tetraanisyl-*para*-phenylenediamine (TAPD) were recorded as the reference

compounds of **5**. The observed absorption and fluorescence spectra of **4**, **5**, and TAPD in THF are summarized in Fig. 8. Compounds **4**, **5**, and TAPD have similar absorption maxima around 310 nm (**4**: λ_{abs} = 312 nm (3.97 eV), **5**: λ_{abs} = 315 nm (3.94 eV), and TAPD: λ_{abs} = 310 nm (4.00 eV)). Photoexcitation at 310 nm (4.00 eV) of these compounds gave weak emissions (**4**: λ_{em} = 412 nm (3.01 eV), Φ = 0.029, **5**: λ_{em} = 442 nm (2.81 eV), Φ = 0.035, and TAPD: λ_{em} = 416 nm (2.98 eV), Φ = 0.032). Although **4** and TAPD showed similar emission maxima, the emission maximum of **5** was red-shifted by 30 nm (200 meV) and 26 nm (170 meV) relative to those of **4** and TAPD, respectively. These results suggest the presence of excimer-like state in **5**, which was reported in the case of oligo(phenylene ethynylene) dimers which are π-stacked by a [2.2]paracyclophane linker.[55]

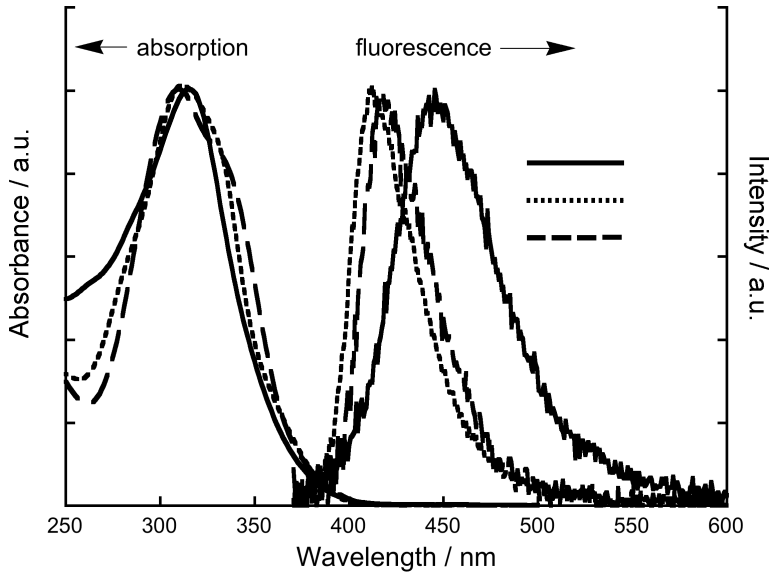

Fig. 8 Absorption and fluorescence spectra of **4** (dotted line), **5** (solid line) and TAPD (broken line) in THF at 298 K.

Conclusions

This work demonstrated that the smallest macrocyclic oligoarylamine (**5**) bearing the alternant *ortho*-*para*-linkage is regarded as a unique compound, in which two redox-active *para*-phenylenediamine (*para*-PD) units are tethered by the two *ortho*-phenylene π-bridges, and therefore, the short contact (less than twice the van der Waals radius of a carbon atom (3.4Å)) between two *para*-phenylene rings is secured, thus strongly suggesting that both through-bond and through-space interactions take an active role in electronic structure of the radical cation ($\mathbf{5}^{\bullet+}$). The ESR study clarified the coexistence of two types of the mixed-valence states in $\mathbf{5}^{\bullet+}$: (i) the statically delocalized mixed-valency within the charged *para*-PD unit and (ii) the dynamically delocalized mixed-valency between the neutral and charged *para*-PD units. Moreover, the dication ($\mathbf{5}^{2+}$) exhibited a diamagnetic closed-shell electronic structure, which is explainable by the McConnell-I model or the topological spin-alignment model in the molecule-based magnetism.

Acknowledgements

This work was partly supported by a Grant-in-Aid for Scientific Research (B) (No. 24310090) from the Japan Society for the Promotion of Science (JSPS) and by a Grant-in-Aid for Scientific Research on Innovative Areas, "New Polymeric Materials Based on Element-Blocks (No. 2401)" (Nos. 24102014 and 25102516) from the Ministry of Education, Culture, Sports, Science, and Technology (MEXT), Japan. D.S. thanks the JSPS Research Fellowship for Young Scientists.

Notes and references

1 H. Tsue, K. Ishibashi and R. Tamura, *Top. Heterocycl. Chem*., 2008, **17**, 73.

2 M.-X. Wang, *Chem. Commun*., 2008, 4541.

3 A. Ito and K. Tanaka, *Pure Appl. Chem*., 2010, **82**, 979.

4 M.-X. Wang, *Acc. Chem. Res*., 2012, **45**, 182.

5 P. Bujak, I. Kulszewicz-Bajer, M. Zagorska, V. Maurel, I. Wielgus and A. Pron, *Chem. Soc. Rev*., 2013, **42**, 8895.

6 J. P. Wolfe, S. Wagaw, J. F. Marcoux and S. L. Buchwald, *Acc. Chem. Res*., 1998, **31**, 805.

7 J. F. Hartwig, *Acc. Chem. Res*. 1998, **31**, 852.

8 J. F. Hartwig, *Angew. Chem. Int. Ed*., 1998, **37**, 2046.

9 A. R. Muci and S. L. Buchwald, *Top. Curr. Chem*., 2002, **219**, 133.

10 A. Ito, Y. Ono and K. Tanaka, *New J. Chem*., 1998, 779.

11 A. Ito, Y. Ono and K. Tanaka, *J. Org. Chem*., 1999, **64**, 8236.

12 M.-X. Wang, X.-H. Zhang and Q.-Y. Zheng, *Angew. Chem. Int. Ed*., 2004, **43**, 838.

13 M.-X.Wang and H.-B. Yang, *J. Am. Chem. Soc*., 2004, **126**, 15412.

14 S.-Q. Liu, D.-X. Wang, Q.-Y. Zheng and M.-X. Wang, *Chem. Commun*., 2007, 3856.

15 E.-X. Zhang, D.-X. Wang, Q.-Y. Zheng and M.-X. Wang, *Org. Lett*., 2008, **10**, 2565.

16 R. J. Bushby, C. A. Kilner, N. Taylor and M. E. Vale, *Tetrahedron*, 2007, **63**, 11458.

17 M. Vale, M. Pink, S. Rajca and A. Rajca, *J. Org. Chem*., 2008, **73**, 27.

18 K. Ishibashi, H. Tsue, N. Sakai, S. Tokita, K. Matsui, J. Yamauchi and R. Tamura, *Chem. Commun*., 2008, 2812.

19 A. Ito, S. Inoue, Y. Hirao, K. Furukawa, T. Kato and K. Tanaka, *Chem. Commun*., 2008, 3242.

20 M. Touil, M. Lachkar and O. Siri, *Tetrahedron Lett*., 2008, **49**, 7250.

21 H. Konishi, S. Hashimoto, T. Sakakibara, S. Matsubara, Y. Yasukawa, O. Morikawa and K. Kobayashi, *Tetrahedron Lett*., 2009, **50**, 620.

22 M. Touil, M. Elhabiri, M. Lachkar and O. Siri, *Eur. J. Org. Chem*., 2011, 1914.

23 A. Ito, Y. Yokoyama, R. Aihara, K. Fukui, S. Eguchi, K. Shizu, T. Sato and K. Tanaka, *Angew. Chem. Int. Ed*., 2010, **49**, 8205.

24 K. Tsuchiya, H. Miyaishi and K. Ogino, *Chem. Lett*., 2011, **40**, 931.

25 A. M. Panagopoulos, M. Zeller and D. P. Becker, *J. Org. Chem*., 2010, **75**, 7887.

26 A. Ito, Y. Ono and K. Tanaka, *Angew. Chem. Int. Ed*., 2000, **39**, 1072.

27 T. D. Selby and S. C. Blackstock, *Org. Lett*., 1999, **1**, 2053.

28 S. I. Hauck, K. V. Lakshmi and J. F. Hartwig, *Org. Lett*., 1999, **1**, 2057.

29 X. Z. Yan, J. Pawlas, T. Goodson, III and J. F. Hartwig, *J. Am. Chem. Soc*., 2005, **127**, 9105.

30 A. Ito, Y. Yamagishi, K. Fukui, S. Inoue, Y. Hirao, K. Furukawa, T, Kato and K, Tanaka, *Chem. Commun*., 2008, 6573.

31 I. Kulszewicz-Bajer, V. Maurel, S. Gambarelli, I. Wielgus, D. Djurado, *Phys. Chem. Chem. Phys*., 2009, **11**, 1362.

32 M. Touil, J.-M. Raimundo, M. Lachkar, P. Marsal and O. Siri, *Tetrahedron*, 2010, **66**, 4377.

33 D. Sakamaki, A. Ito, K. Furukawa, T. Kato and K. Tanaka, *J. Org. Chem*., 2013, **78**,

2947.

34 Alternate *ortho-meta-ortho-meta-* and *meta-meta-para-para*-linked tetraaza[1_n]cyclophanes have been reported so far: see, R. Haddoub, M. Touil, J.-M. Raimundo and O. Siri, *Org. Lett*., 2010, **12**, 2722.

35 H. Hope, J. Bernstein and K. N. Trueblood, *Acta Cryst B*, 1972, **28**, 1733.

36 P. K. Gantzel and K. N. Trueblood, *Acta Cryst*., 1965, **18**, 958.

37 K. Sako, T. Meno, H. Takemura, T. Shinmyozu and T. Inazu, *Chem. Ber*., 1990, **123**, 639.

38 M. V. Baker, M. J. Bosnich, D. H. Brown, L.T. Byrne, V. J. Hesler, B. W. Skelton, A. H. White and C. C. Williams, *J. Org. Chem*., 2004, **69**, 7640.

39 J. Sandström, *Dynamic NMR Spectroscopy*, Academic Press, New York, 1982.

40 H. Sakurai, T. Daiko and T. Hirao, *Science*, 2003, **301**, 1878.

41 The full geometry optimizations of a model compound **5**', **5**'$^{\bullet+}$ and **5**'$^{2+}$ were performed by using Gaussian09 program package: Gaussain09 (Revision C.01), M. J. Frisch et al. Detailed information is given in the ESI.†

42 W. J. Hehre, L. Radom, P. v. R. Schleyer and J. A. Pople, *Ab Initio Molecular Orbital Theory*, Wiley, New York, 1986.

43 Y. Zhao and D. G. Truhler, *J. Phys. Chem*., 2006, **110**, 5121.

44 J.-D. Chai and M. Head-Gordon, *Phys. Chem. Chem. Phys*., 2008, **10**, 6615.

45 J. P. Perdew, K. Burke and Y. Wang, *Phys. Rev. B*, 1996, **54**, 16533.

46 S. H. Vosko, L. Wilk and M. Nusair, *Can. J. Phys*., 1980, **58**, 1200.

47 G. F. Caramori, S. E. Galembeck and K. K. Laali, *J. Org. Chem*., 2005, **70**, 3242.

48 A. S. Jalilov, G. Li, S. F. Nelsen, I. A. Guzei and Q. Wu, *J. Am. Chem. Soc*., 2010, **132**, 6176.

49 A. D. Becke, *J. Chem. Phys*., 1993, **98**, 5648.

50 A. Dreuw and M. Head-Gordon, *Chem. Rev*., 2005, **105**, 4009.

51 J. Hankache and O. S. Wenger, *Chem. Rev*., 2011, **111**, 5138.

52 A. Heckmann, C. Lambert, *Angew. Chem. Int. Ed*., 2012, **51**, 326.

53 A. Rajca, *Chem. Rev*., 1994, **94**, 871.

54 J. A. Crayston, J. N. Devine and J. C. Walton, *Tetrahedron*, 2000, **56**, 7829.

55 S. Mukhopadhyay, S. P. Jagtap, V. Coropceanu, J.-L. Brédas and D. M. Collard, *Angew. Chem. Int. Ed*., 2012, **51**, 11629.

The table of contents

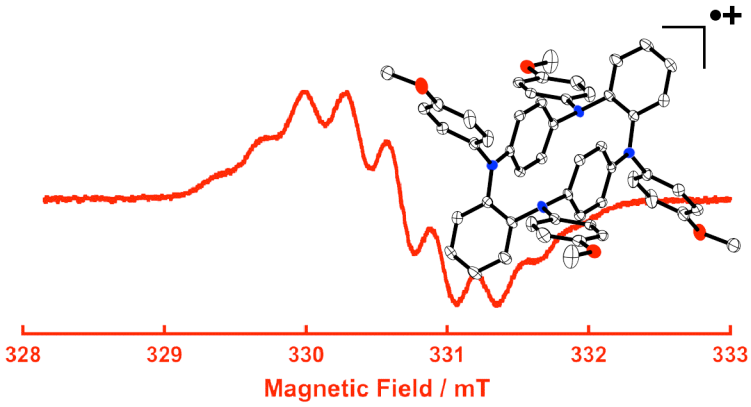

The smallest macrocyclic oligoarylamine bearing the alternant *ortho-para*-linkage exhibits the unique structural and electronic features.